AFRL-VA-WP-TP-2002-316

FOOTPRINT DETERMINATION FOR REUSABLE LAUNCH VEHICLES EXPERIENCING CONTROL EFFECTOR FAILURES

David B. Doman and Anhtuan D. Ngo

JUNE 2002

Approved for public release; distribution is unlimited.

AIR VEHICLES DIRECTORATE
AIR FORCE RESEARCH LABORATORY
AIR FORCE MATERIEL COMMAND
WRIGHT-PATTERSON AIR FORCE BASE, OH 45433-7542

REPORT DOCUMENTATION PAGE

Form Approved
OMB No. 0704-0188

1. REPORT DATE *(DD-MM-YY)*	2. REPORT TYPE	3. DATES COVERED *(From - To)*
June 2002	Journal Article Preprint	Final, 07/01/2001 – 03/31/2002

4. TITLE AND SUBTITLE

FOOTPRINT DETERMINATION FOR REUSABLE LAUNCH VEHICLES EXPERIENCING CONTROL EFFECTOR FAILURES

5a. CONTRACT NUMBER
In-house

5b. GRANT NUMBER

5c. PROGRAM ELEMENT NUMBER
61102F

6. AUTHOR(S)
David B. Doman and Anhtuan D. Ngo

5d. PROJECT NUMBER
2304

5e. TASK NUMBER
F2

5f. WORK UNIT NUMBER
01

7. PERFORMING ORGANIZATION NAME(S) AND ADDRESS(ES)

Control Theory Optimization Branch (AFRL/VACA)
Control Sciences Division
Air Vehicles Directorate
Air Force Research Laboratory, Air Force Materiel Command
Wright-Patterson Air Force Base, OH 45433-7542

8. PERFORMING ORGANIZATION REPORT NUMBER
AFRL-VA-WP-TP-2002-316

9. SPONSORING/MONITORING AGENCY NAME(S) AND ADDRESS(ES)
AIR VEHICLES DIRECTORATE
AIR FORCE RESEARCH LABORATORY
AIR FORCE MATERIEL COMMAND
WRIGHT-PATTERSON AIR FORCE BASE, OH 45433-7542

10. SPONSORING/MONITORING AGENCY ACRONYM(S)
AFRL/VACA

11. SPONSORING/MONITORING AGENCY REPORT NUMBER(S)
AFRL-VA-WP-TP-2002-316

12. DISTRIBUTION/AVAILABILITY STATEMENT
Approved for public release; distribution is unlimited.

13. SUPPLEMENTARY NOTES

Article to be published August 5, 2002 in *Proceedings of AIAA-GNC.*

14. ABSTRACT

The ability to compute the maximum area on the earth's surface (footprint) reachable by an autonomous air vehicle can be useful in planning for the vehicle's safe operations. The information can be important when the vehicle experiences subsystem failures causing it to be unable to maintain its nominal performance. In this paper, we present a method to calculate the footprint of a reusable launch vehicle that experiences a failure in one or more of its aero-control surfaces. During a control effector failure, the maximum attainable moments of the vehicle are reduced, which may decrease the range of conditions that the vehicle can maintain a trimmed condition. Additionally, the lift and drag characteristics of the vehicle can change when control effectors are moved to off-nominal positions to correct for moment imbalance caused by failures or damage. As a result, the footprint of the vehicle is reduced. A technique for calculating the available effectiveness of the aero-control surfaces is used in conjunction with a footprint generation algorithm to include the effects of rotational trim on the vehicle footprint.

15. SUBJECT TERMS

16. SECURITY CLASSIFICATION OF:			17. LIMITATION OF ABSTRACT:	18. NUMBER OF PAGES	19a. NAME OF RESPONSIBLE PERSON (Monitor)
a. REPORT	b. ABSTRACT	c. THIS PAGE			David Doman
Unclassified	Unclassified	Unclassified	SAR	14	19b. TELEPHONE NUMBER *(Include Area Code)* (937) 255-8451

HES&S 31-15093-1

Standard Form 298 (Rev. 8-98)
Prescribed by ANSI Std. Z39-18

AIAA 2002-3463

Footprint Determination for Reusable Launch Vehicles Experiencing Control Effector Failures

Anhtuan D. Ngo and David B. Doman
Air Force Research Laboratory/VACA
2210 Eighth Street, Bldg 146
Wright-Patterson AFB, OH. 45433-7531
Email: anhtuan.ngo@afrl.af.mil/david.doman@wpafb.af.mil

Abstract

The ability to compute the maximum area on the earth's surface (footprint) reachable by an autonomous air vehicle can be useful in planning for the vehicle's safe operations. The information can be important when the vehicle experiences subsystem failures causing it to be unable to maintain its nominal performance. In this paper, we present a method to calculate the footprint of a reusable launch vehicle that experiences a failure in one or more of its aero-control surfaces. During a control effector failure, the maximum attainable moments of the vehicle are reduced which may decrease the range of conditions that the vehicle can maintain a trimmed condition. Additionally, the lift and drag characteristics of the vehicle can change when control effectors are moved to off-nominal positions to correct for moment imbalance caused by failures or damage. As a result, the footprint of the vehicle is reduced. A technique for calculating the available effectiveness of the aero-control surfaces is used in conjunction with a footprint generation algorithm to include the effects of rotational trim on the vehicle footprint.

1 Introduction

Future space operation vehicles aim to achieve affordable and reliable access to space by minimizing the weight and number of subsystems and fluids used in the vehicle. This effort has produced a number of advances in propulsion, structures, materials, and system guidance and control for reusable launch vehicles. Because of the high cost penalty for additional weight, it is desirable for autonomous hypersonic vehicles to have limited hardware redundancy. As a result, the system reliability and safety associated with hardware redundancy may be greatly reduced. Furthermore, control effectors are normally sized to be maximally used during nominal flight conditions so that actuator hardware limits are encountered when one of the actuators fail. Consequently, a single control actuator failure can severely affect the vehicle's performance and safety. To compensate for the reduction in system hardware robustness to control effector failures, attention is being focused on system software by designing guidance and control laws that are adaptive to these failures [1], [2], [3]. Control actuator failures, therefore, along with their effects on mission performance and safety are considered in the whole process of trajectory planning and re-targeting. An important element of the vehicle's safe operation in contingent flying conditions is the ability to compute, in real time, the largest reachable area on the earth's surface given its current conditions, as well as constraints on skin temperature, structural load, and achievable aerodynamics. The reachable area is referred to as the footprint of the vehicle. The footprint information is useful in the event of a system failure and the flight path of the vehicle needs to be altered. In this paper, we apply a technique based on linear optimization with hard constraints on the variables to compute the maximum moments achievable by the vehicle's current control effectors to compute the footprint of a hypersonic vehicle under nominal and contingent operating conditions [5], [6].

2 Problem Formulation

A typical trajectory of a hypersonic vehicle generally consists of five distinct flight segments: ascent, orbit, reentry, terminal area energy management, and approach and landing . Each flight segment is characterized by unique system control settings. Early in the ascent phase, for example, the vehicle experiences low dynamic pressure and relies mainly on propulsive control and thrust vectoring to maintain its attitude and trajectory. Power-pack-out or engine failure is an important control failure to consider during ascent. On

the other hand, during the reentry phase, the propulsion system is normally inactive and not part of the active control effector suite. The aero-control surfaces are the control effectors that are used to direct the vehicle during this phase. This research concentrates on computing the effects of control failures during the reentry phase. The type of failures considered include symmetric effector failure where surfaces are locked in a particular position. In particular, a method for estimating the effect of symmetric failures on force and moment equilibria and the maximum trimmable lift coefficient is presented. The vehicle model used in this study is that of the X-33 shown in Figure 1, which was to be a technology demonstrator for a single stage to orbit spacecraft.

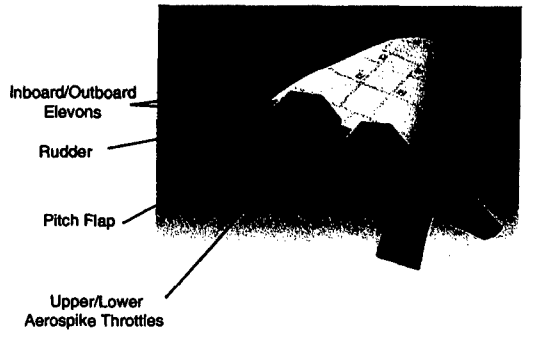

Figure 1: X-33 Reusable Launch Vehicle

2.1 Method for Determining the Range of Trimmable Angles of Attack

We will consider trim conditions where the angular velocity vector is zero. We will therefore neglect the effects of rotational damping, thus, the rolling moment L, pitching moment M, and yawing moment N of the vehicle about its body axes are functions of the angle of attack α, side slip β, altitude h, Mach number M, and control deflection δ:

$$L = L(\alpha, \beta, h, M, \boldsymbol{\delta}) \quad (1)$$
$$M = M(\alpha, \beta, h, M, \boldsymbol{\delta}) \quad (2)$$
$$N = N(\alpha, \beta, h, M, \boldsymbol{\delta}) \quad (3)$$

These moments can be further separated into those generated by the base vehicle configuration, i.e., wing body, propulsion, (L_o, M_o, N_o), and those generated by a suite of m control effectors (L_δ, M_δ, N_δ):

$$L = L_o(\alpha, \beta, h, M) + L_{\boldsymbol{\delta}}(\alpha, \beta, h, M, \boldsymbol{\delta}) \quad (4)$$
$$M = M_o(\alpha, \beta, h, M) + M_{\boldsymbol{\delta}}(\alpha, \beta, h, M, \boldsymbol{\delta}) \quad (5)$$
$$N = N_o(\alpha, \beta, h, M) + N_{\boldsymbol{\delta}}(\alpha, \beta, h, M, \boldsymbol{\delta}) \quad (6)$$

where

$$L_\delta(\alpha, \beta, h, M, \boldsymbol{\delta}) = \Sigma_{i=1}^{m} L_{\delta_i}(\alpha, \beta, h, M, [0 \cdots \delta_i \cdots 0])$$

where $L_{\delta_i}(\alpha, \beta, h, M, \delta_i)$ denotes the rolling moment increment induced by the i^{th} control surface deflected at δ_i. The vehicle's attitude is maintained by the aero-control effectors $\boldsymbol{\delta}$ so that $L = 0$, $M = 0$, $N = 0$ in Equations 4, 5, 6. The calculation of the footprint of the vehicle is then the largest region reachable by the vehicle while still maintaining its desired angular attitude with $L = 0$, $M = 0$, $N = 0$. Under an aero-control effector failure, it is assumed that the configuration-based angular moments L_o, M_o, N_o remained unchanged while the aero-control effectiveness L_δ, M_δ, N_δ are reduced. For the X-33 vehicle with eight aero-control surfaces, it is necessary to calculate the maximum attainable moments achieved by the functioning aero-control effectors. The calculated maximum attainable moments are then used to predict the maximum lift coefficient that is attainable while maintaining rotational equilibrium. Since the maximum attainable moments vary along the vehicle's trajectory, the net moment generating capability of the control effectors must be calculated along the vehicle flight paths that are used to estimate the vehicle footprint. Figure 2 gives an conceptual example of how the attainable moment set might change under a control failure. The maximum attainable moments for a

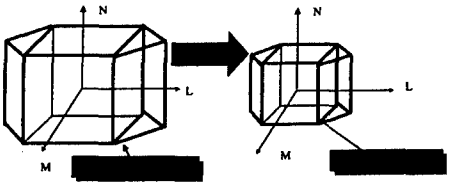

Figure 2: Attainable Moment Sets for a Linear Plant

suite of linear effectors can be calculated by considering the largest moment producing capabilities of a set of control effectors [4]. Since the moment generated by each control surface is a linear function of the surface deflection, the largest moments are found by examining the combined generated moments at the upper and lower limits of their deflection ranges. The geometric envelope of the maximum attainable moments are then represented as facets in the moment space as seen in Figure 2. For a hypersonic vehicle travelling in a dynamic environment, the moments generated by individual control effectors are often nonlinear functions of control deflection. The method presented below considers only symmetric control effector failures.

This condition corresponds to cases where the left and right control surfaces fail in an identical manner so that $L = 0$ and $N = 0$. Such a condition is not as restrictive as it may seem since reconfigurable control laws often balance the lateral moments caused by asymmetric failures by deflecting the opposing control surface to the same (or nearly the same) deflection as the failed surface. For such cases, following method can be used to calculate the attainable moments using the nonlinear aerodynamic database in the pitch axis.

First note that in Equation 5, M_δ can be written as

$$M_{\boldsymbol{\delta}} = \frac{1}{2}\rho v^2 \bar{c} S C_M(\boldsymbol{\delta})$$

where ρ is the air density, v is the velocity, S is the plane form area, $\bar{c}$ is the mean aerodynamic chord, C_{M_δ} is the total control pitching coefficient. The control pitching coefficient can be further expressed as

$$C_{M_{\boldsymbol{\delta}}} = C_{M_{\delta_1}} + \cdots + C_{M_{\delta_m}}$$

The upper bound $\bar{C}_{M_{\boldsymbol{\delta}}}$ and lower bound $\underline{C}_{M_{\boldsymbol{\delta}}}$ of $C_{M_{\boldsymbol{\delta}}}$ can be expressed as

$$\begin{aligned} \bar{C}_{M_{\boldsymbol{\delta}}} &= \bar{C}_{M_{\delta_1}} + \cdots + \bar{C}_{M_{\delta_m}} \\ \underline{C}_{M_{\boldsymbol{\delta}}} &= \underline{C}_{M_{\delta_1}} + \cdots + \underline{C}_{M_{\delta_m}} \end{aligned}$$

where

$$\begin{aligned} \bar{C}_{M\delta_i} &= \max_{\delta_i} C_m(\delta_i) \\ \underline{C}_{M\delta_i} &= \min_{\delta_i} C_m(\delta_i) \end{aligned}$$

Thus, an angle of attack is trimmable if C_{M_o} lies between the upper bound $\bar{C}_{M_{\boldsymbol{\delta}}}$ and lower bound $\underline{C}_{M_{\boldsymbol{\delta}}}$. From figure 3, one can determine that the range of trimmable angles of attack of the X-33 for a flight condition of Mach 12 with the failures of left and right flaps fixed at 10 degrees . The base pitching moments CM_o is bounded by the upper and lower bounds of $C_{\boldsymbol{\delta}}$ for the angles of attack between 17 degrees and 37 degrees. Thus, the set of trimmable angles of attack α_t is defined as $\{\alpha | 17° \leq \alpha \leq 37°\}$. Using this range of trimmable angles of attack, we can then find the condition in which the vehicle is trimmed in its angular attitude, balanced with lift being equal to its weight, and encounters the least drag. In the next section, we will see how these factors affect the vehicle reachable region under no power.

2.2 Footprint Calculation

Assuming that the vehicle angular orientation is maintained by its inner loop attitude controller, the motion of the un-powered vehicle over a non-rotating earth can then be modelled as a point mass:

$$\dot{h} = v\sin(\gamma) \tag{7}$$

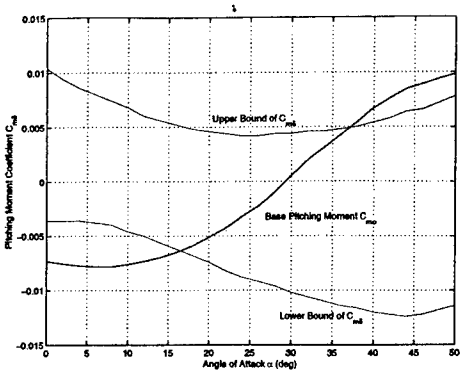

Figure 3: X-33 Pitching Moments at Mach 12

$$\dot{\theta} = \frac{v\cos(\gamma)\cos(\psi)}{(R_o + h)} \tag{8}$$

$$\dot{\phi} = \frac{v\cos(\gamma)\sin(\psi)}{(R_o + h)} \tag{9}$$

$$\dot{v} = \frac{-D}{m} - \frac{\mu\sin(\gamma)}{(R_o + h)^2} \tag{10}$$

$$\dot{\gamma} = \frac{L\cos(\sigma)}{mv} - \frac{\mu\cos(\gamma)}{v(R_o + h)^2} + \frac{v\cos(\gamma)}{(R_o + h)} \tag{11}$$

$$\dot{\psi} = \frac{L\sin(\sigma)}{mv\cos(\gamma)} - \frac{v\cos(\gamma)\cos(\psi)\tan(\phi)}{(R_o + h)} \tag{12}$$

Where

h	:	Altitude
θ	:	Longitude
ϕ	:	Latitude
v	:	Velocity
γ	:	Flight path angle
ψ	:	Heading angle
m	:	Mass of the vehicle
R_o	:	Earth's Radius
μ	:	Gravitational Parameter

The total energy of the un-powered vehicle is strictly decreasing because the non-conservative forces, such as the aerodynamic drag forces and friction, are acting on the vehicle. The vehicle footprint then consists of points on the earth' surface at which the total energy decreases to a set value. When its energy reaches this value, the vehicle then enters the final part of its trajectory called terminal area energy management phase. Combining its velocity v and altitude h in an energy-state approximation [7], a reduced order model can be obtained to simplify the vehicle description. The specific energy of the vehicle can be expressed as

$$E = \frac{1}{2}v^2 + \frac{\mu}{(R_o + h)^2}h \tag{13}$$

From equations 7, 10, and 13, the rate of decrease in the vehicle's energy is

$$\frac{dE}{dt} = -\frac{vD}{m} - \frac{2\mu h v \sin(\gamma)}{(R_o+h)^3} < 0 \qquad (14)$$

Assuming that the vertical forces acting on the vehicles are in equilibrium and its vertical motion frequency dynamics are much faster its horizontal motion dynamics, the flight path angle can be taken to be near zero, i.e., $\gamma \approx 0$. Moreover, since the acceleration normal to the velocity vector is small, i.e., $(v\dot{\gamma} \approx 0)$ and $v \neq 0$, the time-rate of change of the flight path angle can then be taken to be essentially zero, i.e., $\dot{\gamma} \approx 0$. From equation 11, we have

$$L = \frac{m}{cos(\sigma)}\left(\frac{\mu}{(R_o+h)^2} - \frac{v^2}{(R_o+h)}\right) \qquad (15)$$

With

$$L = \frac{1}{2}\rho v^2 S_a C_L \qquad (16)$$

$$D = \frac{1}{2}\rho v^2 S_a C_D, \text{ and } C_D = C_{D_o} + kC_L^2 \qquad (17)$$

we can combine equations 15 and 16 into equation 17 to get

$$D = \frac{1}{2}\rho v^2 S_a C_{D_o} + \frac{2m^2 k\tilde{g}^2}{\rho v^2 S_a \cos^2\sigma} \qquad (18)$$

where $\tilde{g}$ is the effective gravity constant:

$$\tilde{g} = \frac{\mu}{R_o+h} - \frac{v^2}{R_o+h}$$

Given the initial velocity $v(t_o) = v_o$, and initial altitude $h(t_o) = h_o$, the vehicle specific energy $E(t)$ can be calculated according equation 14:

$$E(t) = E_o + dE = \frac{1}{2}v_o^2 + \frac{\mu h_o}{(R_o+h)^2} + dE \qquad (19)$$

The vehicle's velocity $v(t)$ can be derived from the current specific energy $E(t)$:

$$v(t) = \sqrt{2E(t) - \frac{\mu h}{(R_o+h)^2}} \approx \sqrt{2E(t)} \qquad (20)$$

since the vehicle flight altitude h is small when compared to the earth's radius R_o. From the above discussion, the unpowered vehicle under energy-state approximations has the reduced-order model $\dot{x} = f(x,u,t)$ of the form:

$$\dot{\theta} = \frac{v\cos(\psi)}{(R_o+h)\cos(\phi)} \qquad (21)$$

$$\dot{\phi} = \frac{v\sin(\psi)}{R_o+h} \qquad (22)$$

$$\dot{\psi} = \frac{z\tilde{g}}{v} - \frac{v\cos(\psi)\tan(\phi)}{R_o+h} \qquad (23)$$

$$\dot{E} = \frac{-Dv}{m} \qquad (24)$$

where $x = [\theta,\ \phi,\ \psi,\ E]^T$ is the vehicle state vector. The control inputs $u = [\rho\ z]^T$ are the air density, $\rho = \rho(h)$, and the tangent of the bank angle, $z = \tan(\sigma)$. The optimization objective is to find the control vector $u = [\rho\ \ z]$ such that, at time $t = t_f$, the crossrange position specified by the vehicle latitude $\phi(t_f)$ is maximized for a given downrange value $\theta_f = \theta(t_f)$:

$$\max_{\rho,\,z} J = \int_{t_o}^{t_f} G\,dt = \int_{t_o}^{t_f} -\dot{\phi}\,dt \qquad (25)$$

The initial values of the vehicle states are taken to be $\theta(t_o) = 0$, $\phi(t_o) = 0$, $\psi(t_o) = 0$ and $E(t_o) = E_o$.

The Hamiltonian function H to be minimized is

$$H = G + \lambda^T f \qquad (26)$$

$$= -\dot{\phi} + \lambda_\theta\dot{\theta} + \lambda_\phi\dot{\phi} + \lambda_\psi\dot{\psi} + \lambda_E\dot{E} \qquad (27)$$

The weighting coefficients λ are the Lagrangian multipliers to be determined. The necessary conditions for optimality are

$$\frac{\partial H}{\partial x} = -\frac{d\lambda}{dt} \qquad (28)$$

$$\frac{\partial H}{\partial u} = 0 \qquad (29)$$

Taking variations of the Hamiltonian function H, enforcing the condition $\partial H = 0$ at the stationary point of H, and the Lagrangian multipliers do not vary at the boundary produces

$$[H\delta\, t - \lambda^T\delta]_{t_o}^{t_f} = 0$$

The final heading $\psi(t_f)$, the final down-range position $\theta(t_f)$ are unspecified. The initial and final values for the Lagragian multipliers $\lambda(t_o)$ are chosen to be zero. The dynamics of $\lambda(t)$ for $t_o < t < t_f$ can be found from equations 28:

$$\dot{\lambda}_\psi = -\frac{\partial H}{\partial\psi},\ \ \dot{\lambda}_E = -\frac{\partial H}{\partial E}$$

$$\dot{\lambda}_\theta = -\frac{\partial H}{\partial\theta},\ \ \dot{\lambda}_\phi = -\frac{\partial H}{\partial\phi}$$

Combining with equation 24, it can be shown that

$$\lambda_\theta(t) = 0 \qquad (30)$$

$$\lambda_\phi(t) = 1 - \cos(\theta_f - \theta) \qquad (31)$$

$$\lambda_\psi(t) = -cos(\phi)\sin(\theta_f - \theta) \qquad (32)$$

$$\lambda_E(t) = \frac{H_r}{\dot{E}} = \frac{\lambda_\theta\dot{\theta} + \lambda_\phi\dot{\phi} + \lambda_\psi\dot{\psi}}{\dot{E}} \qquad (33)$$

At the optimal control u_{opt}, $H(x,u_{opt},\lambda,t) = 0$ and

$$H(x,u_{opt},\lambda,t) \leq H(x,u_{opt}+\Delta u,\lambda,t) \qquad (34)$$

that is,

$$H_r(x, u_{opt}, \lambda, t) + \lambda_E \dot{E}(x, u_{opt}, \lambda, t) \leq H_r(x, u_{opt} + \Delta u, \lambda, t) + \lambda_E \dot{E}(x, u_{opt} + \Delta u, \lambda, t). \quad (35)$$

From equations 33 and 34, it can be shown that Substituting

$$\lambda_E(t) = \frac{H_r(x, u_{opt}, \lambda, t)}{\dot{E}(x, u_{opt}, t)}$$

into equation 35, we have

$$\frac{H_r(x, u_{opt}, \lambda, t)}{\dot{E}(x, u_{opt}, \lambda, t)} - \frac{H_r(x, u_{opt} + \Delta u, \lambda, t)}{\dot{E}(x, u_{opt} + \Delta u, \lambda, t)} \leq 0 \quad (36)$$

From expression 36, we can define a new Hamiltonian function that relates the vehicle states x, its co-states λ, control u to its decreasing rate of energy $\dot{E}$:

$$H_{new} = \frac{H_r}{\dot{E}} = \frac{-\dot{\phi} + \lambda_\theta \dot{\theta} + \lambda_\phi \dot{\phi} + \lambda_\psi \dot{\psi}}{\dot{E}} \quad (37)$$

Putting values for the states $\dot{\phi}$, $\dot{\theta}$, $\dot{\psi}$, $\dot{E}$ and their co-states λ_ϕ, λ_θ, λ_ψ into equation 37, we have

$$H_{new} = \frac{\left[\begin{array}{l} \frac{-v\sin(\psi)}{R_o+h} + \lambda_\phi \frac{-v\sin(\psi)}{R_o+h} \\ +\lambda_\psi [z(\frac{\mu}{v(R_o+h)^2} - \frac{v}{R_o+h} - \frac{v\cos(\psi)\tan(\phi)}{R_o+h}] \end{array}\right]}{-v(\frac{.5v^2 S_a C_{do}\rho}{m} + \frac{2mk\tilde{g}^2(1+z^2)}{\rho S_a v^2})} \quad (38)$$

For a decreasing total energy ($\dot{E} < 0$), the new Hamiltonian H_{new} is to be maximized with the control parameters being the air density ρ and the bank angle σ. For a hypersonic vehicle under energy-state approximations, methods suggested by Schultz [5] and Vinh [6] are applied. Since the control parameter ρ does not appear in the numerator of H_{new}, H_{new} is maximized when the air density ρ is minimized. From the drag equation 17, we have

$$\frac{\partial D}{\partial \rho} = 0 \Rightarrow \rho_{opt} = \sqrt{\frac{4m^2 k\tilde{g}^2(1+z^2)}{v^2 S_a C_{do}}} \quad (39)$$

The optimum bank angle σ associated with $z = \tan(\sigma)$ is

$$\frac{\partial H}{\partial z} = 0 \Rightarrow z_{opt} = \frac{\cos(\phi)\sin(\tilde{\theta})(\frac{\mu}{R^2} - \frac{v^2}{R})\frac{R}{v^2}}{\cos(\tilde{\theta})\sin(\psi) - \sin(\phi)\sin(\tilde{\theta})\cos(\psi)} \quad (40)$$

with $\tilde{\theta} = \theta_f - \theta$, $R = R_o + h$. From equations 39 and 40 the final downrange $\theta_f = \theta(t_f)$ of the vehicle is needed a priori to generate an optimal bank angle ϕ_{opt} and altitude $\rho_{opt} = \rho(h)$ to achieve the largest final cross-range $\phi_f = \phi(t_f)$. To generate the vehicle entire footprint, it is suggested in [6] to use the vehicle heading $\psi_o = \psi(t_o)$ as the sweeping parameters: $180° \leq \psi_o \leq 90°$. The intermediate downrange θ'_f and cross-range ϕ'_f are transformed by the coordinate transformation to obtain the final θ_f and ϕ_f:

$$\begin{aligned} \tan(\theta_f) &= \tan(\theta'_f)\cos(\psi'_o) + \frac{\tan(\phi'_f)\sin(\psi'_f)}{\cos(\theta'_f)} \\ \sin(\phi_f) &= \sin(\phi'_f)\cos(\psi'_o) - \sin(\theta'_f)\cos(\phi'_f)\sin(\psi'_f) \end{aligned}$$

Equations 39 and 40 give the optimal cross-range $\phi(t_f)$ for a given downrange θ_f. Iterations on the initial values of θ_f may be necessary so that the initial guess matches the final value $\theta(t_f)$ resulted from the equations 24.

3 Approximate Solution

Online footprint computation using the above method may be slow because iterations on θ_f are necessary. An approximate solution to the maximum crossrange calculation was proposed by Vinh [6] for the optimal bank angle command signal.

$$z_{approx} = \tan\left(\frac{1}{2} e^{\kappa} \arctan(\frac{\cos(\phi)}{\tan(\psi)}) \right) \quad (41)$$

where

$$\kappa = \frac{1}{10\sqrt{k\, C_{do}}}$$

The advantage of this approximate solution is that it does not require an initial guess of $\theta(t_f)$ and subsequent iterations. This bank angle control was demonstrated in [6] with good results.

4 Application to a Reusable Launch Vehicle

In this section, we apply the methods for the footprint calculation to the X-33 reusable launch vehicle. The X-33 is an autonomous, reusable launch vehicle that has two linear aerospike engines and eight aerodynamic control surfaces: inner/outer elevons, rudders, flaps as shown in Figure 1. At the beginning of the reentry phase, the 2500-slug vehicle attains the velocity of 10,000 feet/second at an altitude of 180,000 feet. With this initial energy, the unpowered vehicle's cross-range is calculated until its final energy is equivalent to the energy at the final speed of 2500 feet/second and 50,000 feet of altitude. The air density constraint which is related to thermal constraint on the vehicle is $\rho < 7.397 \times 10^{-5}$slugs/ft^3. Similarly, structure-related air density constraint has an upper limit of 3.981×10^{-5}slugs/ft^3.

An important requirement that must be satisfied in calculating the vehicle footprint is the maintenance of lift to effective-weight equilibrium (L=W) while banking

the vehicle:

$$L = \frac{1}{2}\rho^2 S_a C_L = W = \frac{m\tilde{g}}{\cos(\sigma)}$$

where S_a is vehicle planform area and ρ is the air density. The respective normal and axial force coefficients C_N and C_A obtained from the vehicle's aerodynamic table are transformed into the corresponding lift and drag coefficients C_L and C_D:

$$\begin{aligned} C_L &= \cos(\alpha)C_N - \sin(\alpha)C_A \\ C_D &= \sin(\alpha)C_N + \cos(\alpha)C_A \end{aligned}$$

A root solver based on the Secant method is then used to minimize the residual of $L-W$. As discussed earlier, the new Hamiltonian H_{new} in Equation 37 is optimized when the vehicle's drag is minimized. Scanning the altitude that is 20,000 feet above and below the vehicle's current altitude, we look for the next optimal altitude command that minimizes the vehicle's drag subject to the constraint $L = W$. Once the optimal altitude is found, the bank angle command σ is calculated using Vinh's control law in Equation 41. As shown in Equation 41, the bank angle command is a function of the vehicle's current parasitic drag C_{D_o} coefficient and induced drag parameter k. The parasitic drag coefficient C_{D_o} in Equation 17 for the X-33 vehicle is found from the aerodynamic data table by iterating over the vehicle's angle of attack α at a given Mach number to find the drag coefficient at zero lift:

$$C_D = C_{D_o}|_{C_L(\alpha, Mach)=0}$$

A third-order polynomial expression is then used to parameterize C_{D_o} in terms of the vehicle's velocity to give the following Equation:

$$\begin{aligned} C_{D_o} = &-2.8809 \times 10^{-4}\text{Mach}^3 + 7.4321 \times 10^{-3}\text{Mach}^2 \\ &-6.0914 \times 10^{-2}\text{Mach} + 2.9697 \times 10^{-1} \end{aligned}$$

The parameter k in Equation 17 can be found by looking up the values of the lift and drag coefficients from the vehicle's aerodynamic data table and solving:

$$k = \frac{C_D - C_{D_o}}{C_L^2}$$

5 Rotational Equilibrium Under Failures

In addition to ensuring that the lift on the vehicle equals its weight, rotational equilibrium must also be enforced to maintain the vehicle's attitude. A trim routine is used to find the aero-control positions that are necessary to balance the base pitching moment produced by the wing-body portion of the vehicle. The lateral directional moments resulting from the wing-body portion of the vehicle are assumed to be zero (i.e. an assumption of zero steady-state sideslip and wing-body symmetry). In the trim routine, the roll, pitch and yaw control effectiveness of each aero-control surface at a fixed Mach number and angle of attack is found from the aerodynamic table using small perturbations. With B being the pitch control effectiveness matrix, δ the aero-control deflections and M_o the base pitching moment, a linear programming formulation [3] is used to find δ such that:

$$\begin{aligned} &\min_{\delta} J = \|B\delta - M_o\|_1 \\ &\text{subject to} \quad \underline{\delta} \leq \delta \leq \overline{\delta} \end{aligned} \tag{42}$$

where $\underline{\delta}$ and $\overline{\delta}$ are vectors that represent the lower and upper limits of the control effectors. Control surface failures such as locked control surfaces are accommodated by setting the upper and lower limits for the locked effectors equal to one another. By solving the minimization problem posed in Equation 42, the potentially undesirable moments produced by locked effectors are automatically taken out by the un-failed surfaces whenever it is physically possible to do so. One additional comment regarding Equation 42 is in order. The linear programming problem that is posed, assumes that the moments are linearly related to surface deflections. This is rarely the case in practice and at best, at a particular flight condition, the moments are nonlinear functions of surface deflection and in order to find the deflections that produce a desired moment one must find δ that solves the following equation subject to $\underline{\delta} \leq \delta \leq \overline{\delta}$

$$M_o = f(\delta) \tag{43}$$

In general, if the solution to Equation 42 which we will call δ_{lp} is substituted for δ into Equation 43 one will find that:

$$M_o \neq f(\delta_{lp}) \tag{44}$$

An iterative approach has been developed here that solves multiple linear programming problems. The approach finds a modified value of base pitching moment, namely $M_{o_{mod}}$ that produces a control deflection vector $\delta_{lp_{mod}}$ that produces

$$M_o = f(\delta_{lp_{mod}}) \tag{45}$$

The iterative procedure uses the following update rule to compute $M_{o_{mod}}$.

$$M_{o_{mod_{k+1}}} = M_{o_{mod_k}} + \omega(M_o - f(\delta_{lp_{mod_k}})) \tag{46}$$

where k indicates the kth iteration, and ω is a parameter that affects the convergence properties. As stated previously, a locked control surface can be accommodated directly through the control allocator by setting the upper and lower position limits equal to one another. This ensures that the remaining control surfaces

are used to balance the possibly undesirable effects of the locked surfaces as well as balance the wing-body moments. In most cases, one or more locked surfaces create a condition that requires the free surfaces to move to off-nominal positions to counter undesirable effects of the locked surfaces to maintain rotational equilibrium. This ultimately translates into force perturbations that increase the overall drag on the vehicle and therefore reduces the size of the vehicle footprint.

6 Example: Locked Surfaces

The X-33 aerodynamic model is used in this example to optain representative force and moment data for an RLV. The case under consideration uses the techniques described above to compute footprints under nominal conditions and in the case of right inboard and outboard elevons both locked at -30 degrees. In order to maintain rotational equilibrium, the control allocator automatically deflects the left inboard and outboard elevons to -30 degrees to balance the lateral directional moments and deflects the body flaps to balance the pitching moments produced by the other control surfaces and the wing-body. This trimming operation is performed at each time step at which the equations of motion and control commands are computed, in this case, the integration time is 1 second. Figure 4 compares the footprint of the nominal and failed vehicle and one can see that the failed vehicle footprint is reduced in size. This is because of the increase in drag due to the off-nominal control surface deflections that are required to maintain rotational equilibrium. Figure

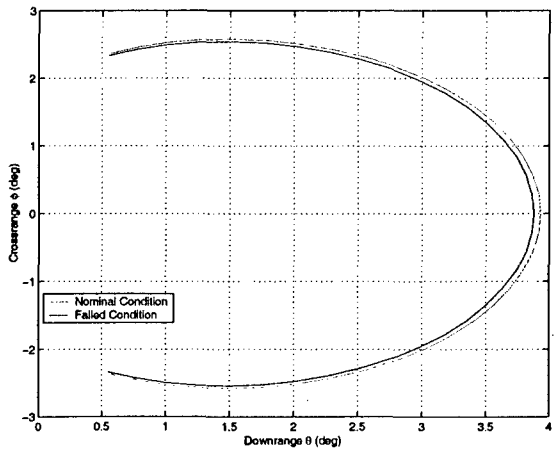

Figure 4: Footprint Comparison between Nominal and Failed Conditions with Right Inboard and Outboard Elevons Locked at $-30°$

5 shows the commanded altitude that yields minimum drag from the initial energy to the final energy to yield the largest crossrange. The discrete profile of commanded altitude arises from the increments used in the altitude sweep. A smoother time history can be obtained by using smaller altitude increments or using results from the coarse sweep to initialize an numerical optimizer to find the altitude at which minimum drag occurs. Using the sweeping method to initialize a numerical optimizer reduces the likelihood of getting trapped at a local minimum. Both approaches result in increased computational time. Figure 6 shows the time history of the bank angle command to achieve the maximum crossrange. The entire footprint of the vehicle is then generated by setting the initial headiang $\psi(t_o)$ from 90 degrees to 0 degree and calculating the vehicle trajectory given the initial and final energies.

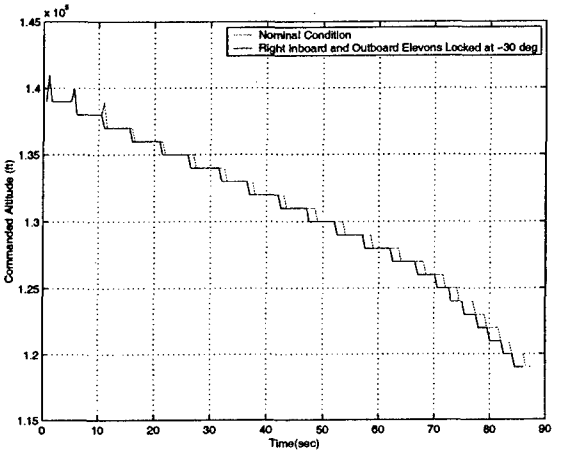

Figure 5: Altitude Command for the Max. Crossrange

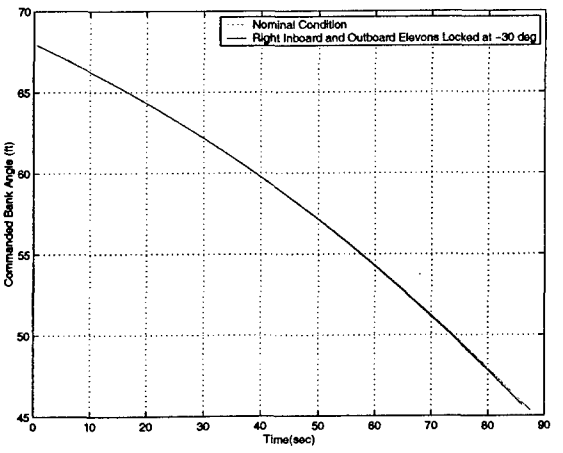

Figure 6: Bank Angle for the Max. Crossrange

7 Effect of Trimmable Angle of Attack

It should be noted that control surface failures can also reduce the range of trimmable angles of attack on some

vehicles. This can cause a maximum wing-body lift coefficients constraint to be replaced by a more conservative maximum trimmable lift coefficient constraint. Whether such constraints become active or not is dependent upon the vehicle; however, loss or damage to any of the aero-control surfaces could potentially reduce the maximum trimmable angle of attack. This reduction can decrease the maximum achievable lift that strongly influences the cross-range that can be achieved by banking the vehicle. In this case studied here, such a constraint was never active because the X-33 requires less control power to trim at high angles of attack than at low angles of attack. Additionally, minimum drag conditions on this vehicle generally occur at high altitude and at high angles of attack. Nevertheless, it is interesting to look at the reduction in the size of the vehicle footprint that would result from a hypothetical reduction in trimmable angle of attack. Such a case can be seen in Figure 7. In calculating the two footprints shown in Figure 7, the vehicle initial conditions remain the same while its maximum trimmable angle of attack is reduced from 50 degrees to 7 degrees.

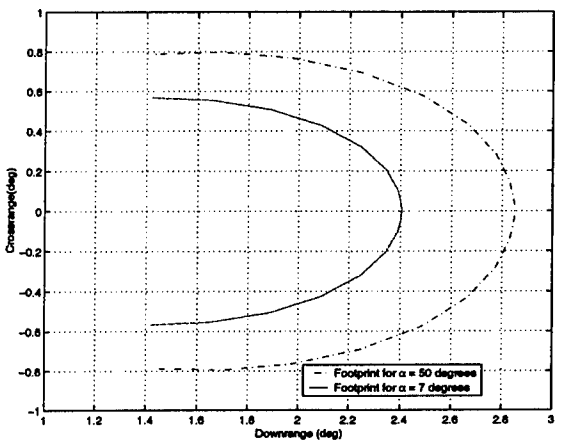

Figure 7: Footprint Sensitivity to Varying Constraints on Max. Angle of Attack

8 Conclusion

In this paper, methods to calculate the largest reachable area are presented. The optimal method is based on variational calculus and requires iterations on the initial guess. The suboptimal method is based on approximations, but is more practical for implementation. A numerical example is used to show how the vehicle's largest reachable area can shrink under failure. Such information can be useful in the process of selecting a safe and available landing site under contingencies.

References

[1] E. N. Johnson, A. J. Calise, E. J. Corban, "Reusable Launch Vehicle adaptive Guidance and Control Using Neural Networks," in *Proceedings of the 2001 Guidance, Navigation and Control Conference*, AIAA 2001-4381, Aug. 2001.

[2] J. D. Schierman, D. G. Ward, J. F. Monaco, J. R. Hull, "A Reconfigurable Guidance Approach For Reusable Launch Vehicles," in *Proceedings of the 2001 Guidance, Navigation and Control Conference*, AIAA 2001-4429, Aug. 2001.

[3] D. B. Doman, A. D. Ngo, D. B. Leggett, M. A. Saliers, "Development of A Hybrid Direct-Indirect Adaptive Control System for the X-33," in *Proceedings of the 2001 Guidance, Navigation and Control Conference*, AIAA 2001-4156, Aug. 2001.

[4] W. C. Durham, "Attainable Moments for the Constrained Control Allocation Problem," *Journal of Guidance, Control, and Dynamics*, Vol. 17, No. 6, 1994, pp. 1371-1373

[5] R. L. Schultz, "Three-Dimensional Trajectory Optimization for Aircraft," *Journal of Guidance, Control and Dynamics*, Vol. 13, No. 6, November - December 1990, pp. 936-943.

[6] N. X. Vinh, *"Optimal Trajectories in Atmospheric Flight,"* Elsevier Scientific Publishing Company.

[7] E. S. Rutowski, "Energy Approach to the General Aircraft Performance Problem," *Journal of Aeronautical Sciences* Vol. 21, 1954, pp. 187-195.